Composite generalized Langevin equation for Brownian motion in different hydrodynamic and adhesion regimes

Hsiu-Yu Yu
Department of Chemical and Biomolecular Engineering and Department of Bioengineering, University of Pennsylvania, Philadelphia, Pennsylvania 19104, USA

David M. Eckmann
Department of Anesthesiology and Critical Care and Department of Bioengineering, University of Pennsylvania, Philadelphia, Pennsylvania 19104, USA

Portonovo S. Ayyaswamy
Department of Mechanical Engineering and Applied Mechanics, University of Pennsylvania, Philadelphia, Pennsylvania 19104, USA

Ravi Radhakrishnan*
Department of Bioengineering and Department of Chemical and Biomolecular Engineering, University of Pennsylvania, Philadelphia, Pennsylvania 19104, USA

(Received 28 January 2015; revised manuscript received 9 February 2015; published 12 May 2015)

We present a composite generalized Langevin equation as a unified framework for bridging the hydrodynamic, Brownian, and adhesive spring forces associated with a nanoparticle at different positions from a wall, namely, a bulklike regime, a near-wall regime, and a lubrication regime. The particle velocity autocorrelation function dictates the dynamical interplay between the aforementioned forces, and our proposed methodology successfully captures the well-known hydrodynamic long-time tail with context-dependent scaling exponents and oscillatory behavior due to the binding interaction. Employing the reactive flux formalism, we analyze the effect of hydrodynamic variables on the particle trajectory and characterize the transient kinetics of a particle crossing a predefined milestone. The results suggest that both wall-hydrodynamic interactions and adhesion strength impact the particle kinetics.

DOI: 10.1103/PhysRevE.91.052303 PACS number(s): 82.70.Dd, 47.11.−j, 47.63.−b, 87.85.gf

I. INTRODUCTION

Describing the motion of nanoparticles is an essential topic in many applications of colloidal hydrodynamics such as targeted drug delivery [1–3], pathogen detection [4,5], quantification of expressed protein expression [6,7], microfluidics-based sorting [8–11], and microrheology of soft matter [12–14]. In such applications, nanoparticles have tailored affinities with the target, and the interplay between hydrodynamic interactions, adhesive interactions, Brownian motion, and other external forces impacts the motion of the nanoparticle across different regimes (see Fig. 1). Direct numerical simulations (DNSs) of fluctuating hydrodynamics equations can resolve the correct hydrodynamic and thermal correlations of the particle over the fluid viscous relaxation time $\tau_\nu = a^2/\nu$ (a being the particle radius and ν the fluid kinematic viscosity) [15–18] but due to computational overhead cannot access pharmacodynamic timescales (ms-hours). Implicit-solvent simulation methods (e.g., Brownian or Stokesian dynamics [19,20]) explore dynamics efficiently over longer diffusive time scales [$O(a^2/D)$ with D being the particle diffusivity]. However, they do not naturally encode the correct temporal correlations over the time scale of τ_ν. To address these limitations, in this article we present a composite generalized Langevin equation (GLE) formalism as a unified framework for resolving the nanoparticle dynamics in the presence of hydrodynamic correlations, thermal motion, and an external potential mimicking binding forces in different hydrodynamic regimes (e.g., bulk, near-wall, and lubrication, as shown in Fig. 1).

GLE is a mathematical construct for the particle equation of motion that incorporates a memory function denoting a systematic resistance and a complementary random fluctuating force. Rigorously, GLE for a Brownian particle near a boundary can be formulated from the Zwanzig-Mori projection formalism [21] with all the hydrodynamic modes accurately included. However, the main difficulty originates from the fact that different hydrodynamic modes correlate at different time scales, especially when boundaries are introduced. In such circumstances, inevitably, relevant approximations for the projection operator and the memory function would be necessary. On the other hand, in the analytical treatment of Felderhof [22], the motion of a Brownian particle near a planar wall is addressed from the perspective of frequency-dependent admittance in the point-particle limit. Although the velocity autocorrelation function may be obtained with a hydrodynamic spectrum in the frequency domain, the time-domain equation of motion for the particle is tractable only in the case without a bounding wall; in the presence of a planar wall, only an approximation to the long-time asymptotic limit can be recovered. Consequently, in this article we apply a physically motivated approach by incorporating the generic hydrodynamic correlations at the relevant time scales into a single composite GLE. For bulk and near-wall regimes, we employ the analytical form of the memory function resulting from the solution of the linearized Navier-Stokes equation

*rradhak@seas.upenn.edu

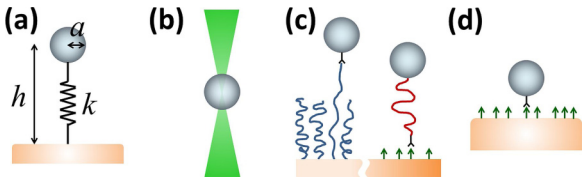

FIG. 1. (Color online) Schematics of a Brownian particle: (a) model of a particle with radius a bound by a spring with the spring constant k at a position h separated from a wall; (b) trapping a particle using optical tweezers (weak harmonic potential with $k \approx 10^{-6}$–10^{-5} N/m [24,26]); (c) ligand-functionalized particle interacting with a polymer tether or polymer-grafted particle binding to receptors on the substrate or cell (near-wall or lubrication regime depending on the ratio of $(h-a)/a$ under a moderately strong harmonic potential with $k \approx 10^{-4}$–10^{-2} N/m [27,28]); (d) nanoparticle of radius $a = 50$–250 nm bound to the cell via antibody-antigen interactions coinciding with the lubrication regime [for molecules of size $O(10\,\text{nm})$, $(h-a)/a \ll 1$], and a strong harmonic potential with $k = 0.1$–1 N/m.

and construct a suitable GLE to incorporate the stochastic effects. For the lubrication regime, we construct a GLE based on transverse lubrication flows within the particle-wall gap. In each case, the transition in the temporal correlations is handled within the composite structure, where for early times a "bulk like" interaction is considered, and for long times the hydrodynamic-wall effect is included. We validate our approach by comparing the computed particle velocity autocorrelation function (VACF) with available analytical solutions for the bulk [23] and near-wall regimes [22,24] and provide new predictions for the lubrication regime. Through analyzing the nanoparticle VACF and position autocorrelation function (PACF) ($C_v = \langle U(t)U(0)\rangle$ and $C_x = \langle \delta x(t)\delta x(0)\rangle$), we demonstrate how one may simultaneously characterize nanoparticle dynamics subject to adhesive interactions and other external forces while incorporating hydrodynamic correlations and maintaining thermal equilibrium in multiple regimes. In order to elucidate the effect of hydrodynamics on activated processes, we analyze particle trajectories to estimate kinetic rates for nanoparticle crossing a predefined milestone using the reactive flux formalism [25].

The remainder of the article is structured as follows: We present our theoretical description of the GLE framework in Sec. II and numerical method in Sec. III followed by results and discussions in Sec. IV. In Sec. IV we validate thermal equilibrium of our stochastic simulations (Sec. IV A), delineate our autocorrelation functions in different hydrodynamic and adhesion regimes (Sec. IV B), and discuss milestoning rates based on dynamical trajectories (Sec. IV C). Finally, conclusions are given in Sec. V.

II. THEORY: THE GLE FRAMEWORK

The translational equation of motion ($m\frac{dU}{dt} = \sum_i F_i$) for a Brownian particle with mass m and velocity U at position x subject to an external harmonic potential force, $F_{\text{ext}}(x) = -kx$, can be cast into a GLE that in one dimension reads

$$M\frac{dU}{dt} = -\int_{-\infty}^{t} \zeta(t-t')U(x,t')\,dt' - kx(t) + R(t), \quad (1)$$

where M is the particle effective mass (described below), $\zeta(t)$ is the frictional memory kernel capturing the hydrodynamic interactions, and $R(t)$ with $\langle R(t)\rangle = 0$ is the thermal fluctuating force on the particle. $\zeta(t)$ and $R(t)$ are linked via the second fluctuation-dissipation theorem [29], $\langle R(t)R(t')\rangle = k_B T\zeta(|t-t'|)$ with Boltzmann constant k_B and temperature T.

The frictional force F_{drag} acting on a Brownian spherical particle in an unbounded, incompressible fluid ("bulk regime") is obtained by solving the time-dependent Stokes equation of an incompressible fluid of density ρ surrounding a no-slip solid particle surface and integrating the resulting hydrodynamic stress on the surface. In the frequency domain, $F_{\text{drag}}(\omega) = -\zeta^*(\omega)U(\omega)$ with the time-dependent drag coefficient $\zeta^*(\omega) = 6\pi\eta a + 6\pi a^2\sqrt{i\omega\rho\eta} + (2/3)\pi a^3 i\omega\rho$ [30–32]. The first term represents the Stokes's friction, the second term arises from the diffusion of fluid momentum around the particle surface, and the third term represents the fluid inertia added to the particle inertia. The resulting equation of motion in the time domain is written as

$$M\frac{dU}{dt} = -6\pi\eta a U(x,t) + 3a^2\sqrt{\pi\rho\eta} \times \int_{-\infty}^{t} |t-t'|^{-\frac{3}{2}} U(x,t')\,dt' - kx(t) + R(t) \quad (2)$$

with $M = m + (2/3)\pi a^3\rho = 3m/2$ and $(2/3)\pi a^3\rho$ being the added mass. Comparing Eqs. (1) and (2) yields $\zeta(t) = 12\pi\eta a\delta(t) - 3a^2\sqrt{\pi\rho\eta}t^{-\frac{3}{2}}$, also suggesting that we may write $R(t) = R_w(t) + R_c(t)$ with a white noise correlation $\langle R_w(t)R_w(t')\rangle = 12\pi\eta a k_B T\delta(t-t')$ and a colored noise correlation $\langle R_c(t)R_c(t')\rangle = -3a^2\sqrt{\pi\rho\eta}k_B T|t-t'|^{-\frac{3}{2}}$, and $\langle R_w(t)R_c(t')\rangle = \langle R_w(t)\rangle\langle R_c(t')\rangle = 0$.

In scenarios depicted in Fig. 1(c), the planar wall causes the hydrodynamic response of the fluid to be altered, which leads to a more complex relaxation spectrum of the particle velocity. Linear hydrodynamics suggests that the particle velocity can be written as a perturbation about the bulk case: $U(x,t) = U_0(x,t) + U'(x,t)$. When the particle is not very close to the wall ("near-wall" regime, $h/a \gg 1$), prior studies for motion perpendicular to the wall [33–35] predicted the correct transient scaling of $C_{v,\perp} \sim t^{-\frac{7}{2}}$ over intermediate times ($\tau_\nu < t \leqslant \tau_w = h^2/\nu$) before the true long-time scaling is observed. Recently, it was indicated by analytical theories [22,24] and optical trap experiments [24,26] that $C_{v,\perp}$ shows a $U_0(x,t)$-dominant $t^{-\frac{3}{2}}$ power-law decay for $\tau_\nu \lesssim t \ll \tau_w$, and a $U'_\perp(x,t)$-dominant anticorrelation $t^{-\frac{5}{2}}$ power-law decay for $t \gg \tau_w$, where the diffusion of fluid momentum is highly impacted by the wall. Although $C_{v,\perp}$ can be obtained through a time-Fourier analysis of the particle equation of motion in the absence of thermal fluctuations [22,24], for purposes of particle tracking, it is desirable to obtain the particle trajectory and directly calculate the correlation functions. In order to bridge the aforementioned hydrodynamic correlations due to $U_0(x,t)$ and $U'_\perp(x,t)$ into a particle equation of motion, at the phenomenological level, we propose a "composite GLE" that explicitly encodes the pertinent time scales using a bridging function. If one solves a Langevin equation with a white noise alone over the characteristic time scale of τ_w, the average velocity would behave as $\sim U(0)e^{-\frac{t}{\tau_w}}$. Therefore, a natural

choice of the bridging function would be $e^{-\frac{t}{\tau_w}}$ and we arrive at

$$M\frac{dU_\perp}{dt} = -6\pi\eta a\beta U_\perp(x,t) - A_1(t)\int_{-\infty}^{t}|t-t'|^{-\frac{3}{2}}U_\perp(x,t')\,dt' - A_2(t)\int_{-\infty}^{t}|t-t'|^{-\frac{5}{2}}U_\perp(x,t')\,dt' - kx(t) + R(t), \tag{3}$$

where $\beta = (1-\frac{9a}{8h})^{-1}$ corrects the $O(a/h)$ enhanced resistivity to the particle motion and denotes Lorentz's steady-state friction coefficient [36]. $M = (3m/2)(1-\frac{a^3}{8h^3})^{-1}$ is obtained from the high-frequency admittance [22,24] and shows how the wall affects the particle effective mass, $A_1(t) = -3a^2\sqrt{\pi\rho\eta}(e^{-\frac{t}{\tau_w}})$ gives the amplitude of the intermediate-time $t^{-\frac{3}{2}}$ correlation, and $A_2(t) = \frac{9}{8}am\sqrt{\frac{\rho}{\pi\eta}}\beta^2(1-e^{-\frac{t}{\tau_w}})$ complements $A_1(t)$ and yields the amplitude of the long-time $t^{-\frac{5}{2}}$ decay. $R(t) = R_w(t) + e^{-\frac{t}{\tau_w}}R_{c1}(t) + (1-e^{-\frac{t}{\tau_w}})R_{c2}(t)$ with $\langle R_w(t)R_w(t')\rangle = 12\pi\eta a\beta k_B T\delta(t-t')$, $\langle R_{c1}(t)R_{c1}(t')\rangle = -3a^2\sqrt{\pi\rho\eta}k_B T|t-t'|^{-\frac{3}{2}}$, $\langle R_{c2}(t)R_{c2}(t')\rangle = \frac{9}{8}am\sqrt{\frac{\rho}{\pi\eta}}\beta^2 k_B T|t-t'|^{-\frac{5}{2}}$, and $\langle R_w(t)R_{c1}(t')\rangle = \langle R_w(t)R_{c2}(t')\rangle = \langle R_{c1}(t)R_{c2}(t')\rangle = 0$. This composite GLE essentially captures the relaxations corresponding to $U_0(x,t)$ for all time scales and $U'_\perp(x,t)$ for long times; we also note that in the limit of $A_2 \to 0$ and $\beta \to 1$ for a particle far from a wall, we recover Eq. (2). We note that this approximation of time-dependent bridging functions makes one use a nonstationary mathematical equation to predict a stationary physical process. Consequently, as will be shown in Sec. III, when calculating all the time correlation functions associated with Eq. (3) we shall not invoke time shifting and reversibility but carefully ensemble-average the trajectories to produce the expected physical results.

As shown in Fig. 1(d), when adhesion is mediated directly via receptor–ligand interactions without tethers such as the case where nanocarriers functionalized with antibodies are bound to the antigens on the surface of biological cells [37], the Brownian particle is extremely close (10–40 nm) to the wall ("lubrication regime") such that $(h-a)/a \ll 1$ with strong viscous resistance to particle motion. Moreover, as $\tau_v \sim \tau_w$, the fluid momentum diffusion is curtailed by confinement, which would result in a faster (exponential) decay in C_v than the algebraic correlation for the near-wall case, making the fluid memory effect negligible over a wide span of t. While theoretical investigations of the VACF in the lubrication regime have not been reported, it has been shown that C_v decays exponentially when a particle is placed between parallel plates where the strong confinement influences the fluid momentum diffusion [38,39]. Therefore, we assume quasisteady state and apply classical lubrication theory, which yields $F_{drag} = -[6\pi\eta a^2/(h-a)]dh/dt$ [40], and arrive at the following approximate equation of motion for the particle:

$$M\frac{dU_\perp}{dt} = -\left[\frac{6\pi\eta a^2}{h(t)-a}\right]U_\perp(x,t) - kx(t) + R(t), \tag{4}$$

where $M = 3m/2$ accounts for the added mass and $\langle R(t)R(t')\rangle = \frac{12\pi\eta a^2 k_B T}{h(t)-a}\delta(t-t')$.

III. NUMERICAL METHOD

The numerical schemes for integrating Eqs. (2)–(4) and random force generation are delineated in the Appendix. In all three cases, we follow the Ito calculus for integrating stochastic differential equations without including the "drift" term due to the spatially dependent ζ. We have confirmed that including the drift term does not lead to a difference in the results. We consider a Brownian particle of $a = 250$ nm initially at $x(0) = 0$ with an initial velocity $U(0)$ released into a quiescent fluid ($\eta = 10^{-3}$ kg/ms, $\rho = 1$ kg/m^3, and $\tau_v = 6.25\times10^{-8}$ s) at $T = 310$ K, and numerically integrate Eqs. (2)–(4) by writing $U = dx/dt$ and expressing time derivatives by a finite difference method. The white noise term of the random force $R(t)$ is obtained by choosing the Gaussian random variable, while the colored noise term is calculated by introducing the desired power-law correlation from the frequency domain [41,42]. The stochastic simulations require a large number of realizations to reach satisfactory statistics of the dynamical properties. Since $\zeta(t)$ is hydrodynamic in origin, the scaled relaxation of $U(t)$ can be obtained in the presence or absence of the random force $R(t)$. Therefore, we also perform deterministic simulations in which the particle is driven initially by a weak impulse giving $U(0)$ in the absence of the random force. Based on Onsager's regression hypothesis [43], the correlation between a macroscopically driven $U(0)$ and the subsequent $U(t)$ would be equivalent to the calculated $C_v(t)$ obtained from the stochastic simulations.

For Eqs. (2) and (4), since the mathematical equations are stationary, the resulting time correlation function $\langle A(t_1)A(t_2)\rangle$ equals $\langle A(t)A(0)\rangle$ as long as $t = t_1 - t_2$. In such a case, we follow the standard ensemble averaging procedure outlined in Ref. [44] with time shifting and reversibility to obtain all the time correlation functions. In our stochastic simulations, 100 to 200 realizations with time steps $N = 10^5$ or 2^{17} and step size $\Delta t = 10^{-10}$ s can yield satisfactory averaging up to $t \sim 5\tau_v$ compared with deterministic simulations. However, for Eq. (3), the bridging functions $e^{-\frac{t}{\tau_w}}$ and $1-e^{-\frac{t}{\tau_w}}$ make the mathematical equation nonstationary. Therefore, when calculating the autocorrelation functions in this case, for a given initial configuration (separation from the wall and position within the harmonic potential) of the particle, we need to take the ensemble average over enough realizations. In each simulation, we allow the initial N_{init} steps for equilibration before analyzing the statistics of particle trajectories. In the results for a particle initially placed at the minimum of the harmonic potential in the near-wall regime, at least 2000 realizations with $N = 2^{14}$, $\Delta t = 10^{-9}$ s, and $N_{init} = 10$ are required to reach satisfactory averaging up to $t \sim \tau_v$. The corresponding $C_x(t)$ therefore yields an average trajectory of the particle initially placed at the minimum of the harmonic potential. Consequently, as will be seen in our results, $C_x(t)$ shows an initial increase and then decreases as the particle velocity changes sign.

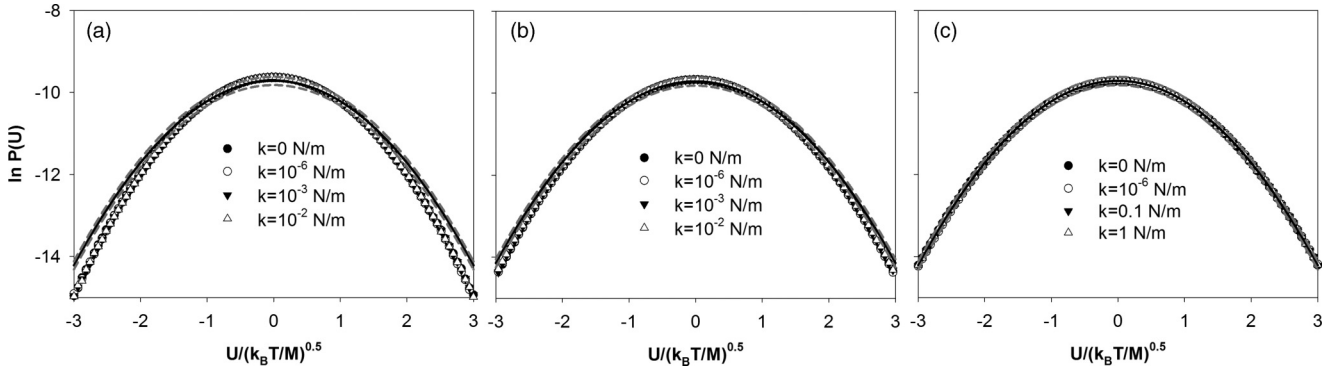

FIG. 2. Equilibrium probability density of the translational velocity, $\ln P(U)$, of the neutrally buoyant nanoparticle (radius $a = 250$ nm) trapped in different harmonic potentials for (a) bulk, (b) near-wall ($h/a = 2$), and (c) lubrication ($h/a = 1.14$) regimes. The solid curves denote the Maxwell-Boltzmann distribution and the dashed curves show 10% error about the Maxwell-Boltzmann distribution.

IV. RESULTS AND DISCUSSION

A. Equilibrium statistics

In our stochastic simulations, the particle temperature agrees satisfactorily with the preset temperature [i.e., within 7% error for Eq. (3) and 0.1% for Eq. (4)]. Figures 2 and 3 present the equilibrium distribution of particle velocity and potential of mean force obtained from the distribution of particle center-of-mass position for various conditions considered in this work. Clearly, the stochastic GLE simulations yield satisfactory equilibrium statistics and reproduce the correct particle configuration. Moreover, the distributions of particle velocity and center of mass are within 10% of the Boltzmann distribution.

Figure 4 shows the nanoparticle mean squared displacement (MSD) for different hydrodynamic and adhesion regimes. For all cases, MSD exhibits a quadratic trend denoting the ballistic motion of a nanoparticle at very short times. For $k = 0$ N/m and $k = 10^{-6}$ N/m, MSD transitions to a purely diffusive behavior within our simulation time, with the slope of MSD being equivalent to the diffusivity, $D = \frac{k_B T}{6\pi\eta a\beta}$. As the harmonic potential is more substantial, MSD gradually plateaus, suggesting the particle is trapped by the potential.

B. Autocorrelation functions

As shown in Fig. 5, for an unbound, neutrally buoyant Brownian particle in a bulk fluid [Eq. (2)], both the normalized $C_v(t)$ from stochastic GLE (100 realizations, $\Delta t = 10^{-10}$ s) and $U(t)/U(0)$ from deterministic GLE ($\Delta t = 10^{-10}$ s) agree remarkably well with the analytical solution of the normalized $C_v(t)$ for particle in a linearized Navier-Stokes

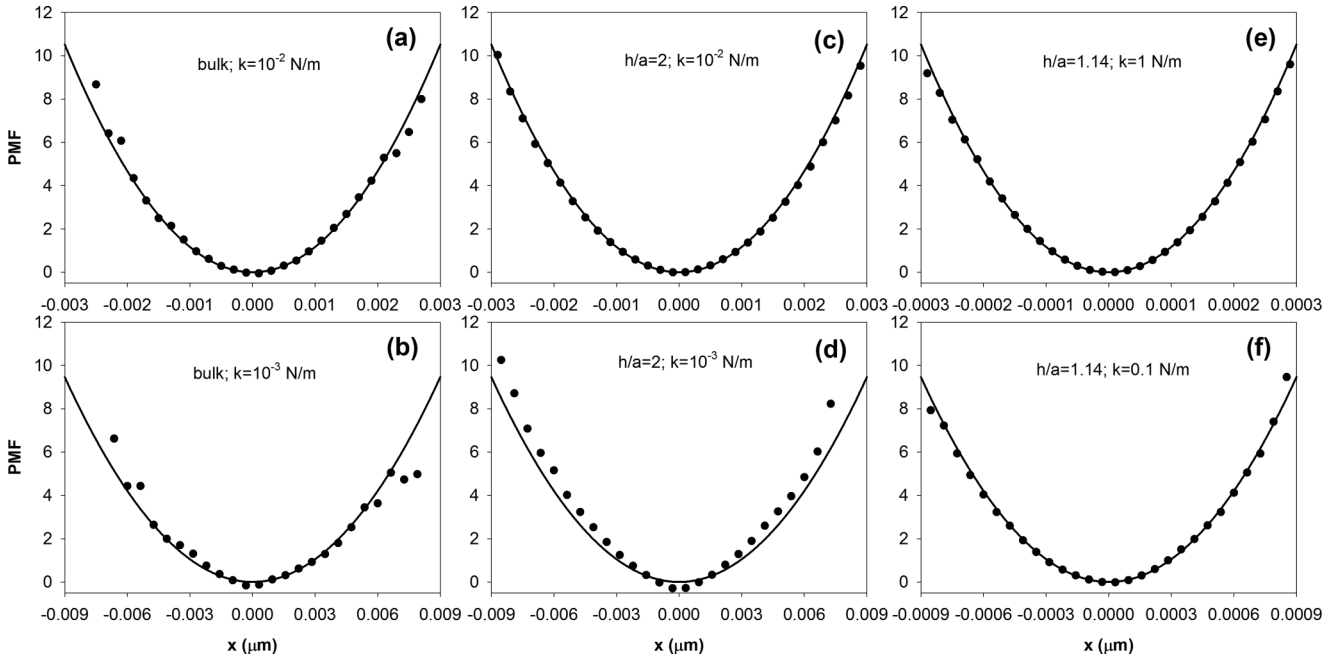

FIG. 3. Equilibrium potential of mean force (PMF), $-\ln P(x)$, of the neutrally buoyant nanoparticle ($a = 250$ nm) trapped in different harmonic potentials for (a, b) bulk, (c, d) near-wall ($h/a = 2$), and (e, f) lubrication ($h/a = 1.14$) regimes. $P(x)$ is the equilibrium probability of the nanoparticle center-of-mass position. The dots are GLE results and the solid curves denote $-\frac{kx^2}{2k_B T}$.

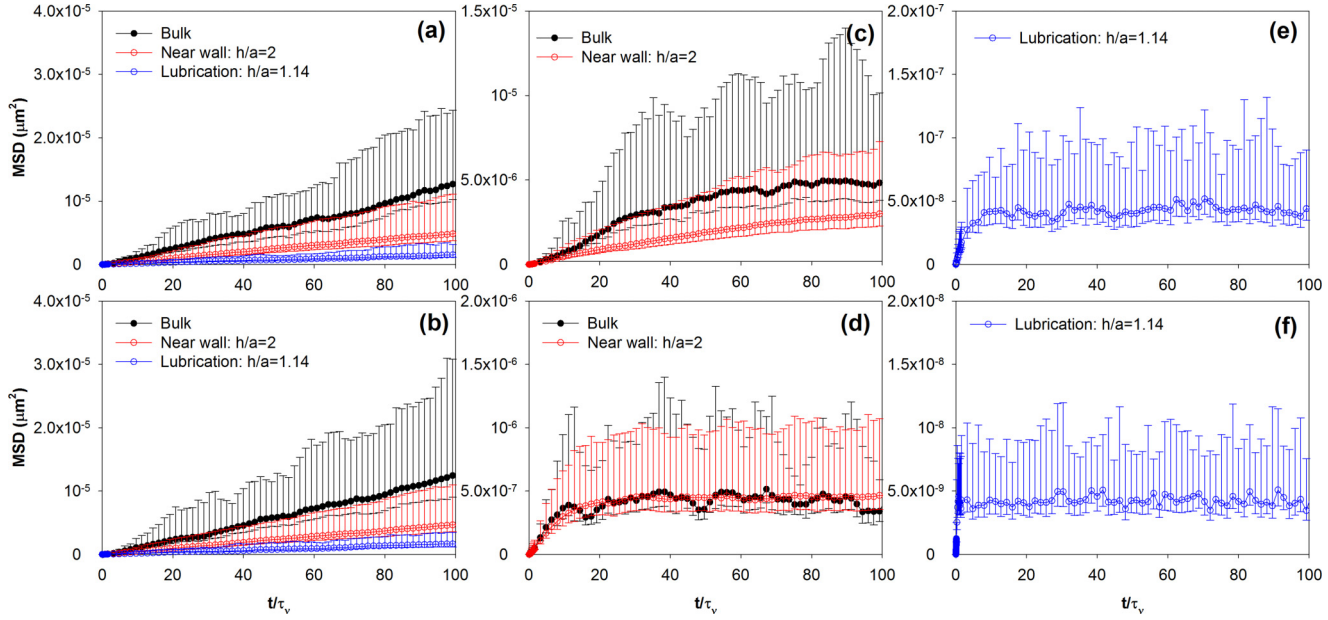

FIG. 4. (Color online) Mean squared displacement with error bars of the neutrally buoyant nanoparticle ($a = 250$ nm) in different hydrodynamic regimes subject to the harmonic potential of (a) $k = 0$ N/m, (b) $k = 10^{-6}$ N/m, (c) $k = 10^{-3}$ N/m, (d) $k = 10^{-2}$ N/m, (e) $k = 0.1$ N/m, and (f) $k = 1$ N/m as will be shown in Fig. 7.

fluid [23]. Specifically, $C_v(t)$ shows an initial exponential decay at short times ($t \ll \tau_\nu$) due to the instantaneous fluid resistance ($6\pi\eta a$). This is followed by a $t^{-3/2}$ algebraic decay at times longer than the viscous relaxation time; that is, for $t \geqslant \tau_\nu$, $C_v(t)$ merges with a $t^{-3/2}$ algebraic decay characterizing the long-time tail resulted from the fluid vortex diffusion.

In Fig. 6, we validate our composite GLE [Eq. (3)] by comparing $C_v(t)$ [or $U(t)/U(0)$] from the deterministic GLE ($\Delta t = 10^{-9}$ s) with the normalized $C_v(t)$ from Ref. [24] which includes the full velocity correlation spectrum for a slightly denser particle at different distances from the wall. Following the initial exponential decay, C_v first shows a $t^{-3/2}$ scaling over $t \sim \tau_\nu$ and dictates a faster decay (approximately $t^{-7/2}$) that deviates from $t^{-3/2}$ scaling as $t \sim \tau_w$. This faster intermediate decay denotes the appearance of wall reflection for the vortex diffusion, which eventually yields the anticorrelation (oscillation) followed by a final long-time $t^{-5/2}$ scaling as $t \gg \tau_w$. Remarkably, the result predicted by the composite GLE for $h/a = 2$ agrees closely with the literature result. Consistent with Ref. [24], the anticorrelation in C_v occurs at an earlier time for smaller h/a, and the long-time $t^{-5/2}$ decay is nearly independent of h/a, as the coefficient A_2 in Eq. (3) also suggests.

In Fig. 7, the normalized $C_v(t)$ and $C_x(t)$ from both stochastic and deterministic simulations are compared in the

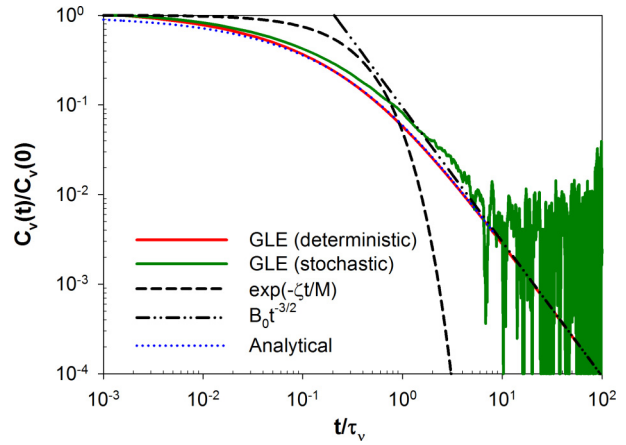

FIG. 5. (Color online) Normalized VACF of a neutrally buoyant Brownian particle in an incompressible, quiescent, unbounded fluid medium obtained from the stochastic and deterministic GLE [Eq. (2)]. The short-time exponential correlation, the long-time algebraic decay, and the full analytical solution of linearized Navier-Stokes equations [23] are shown for comparison.

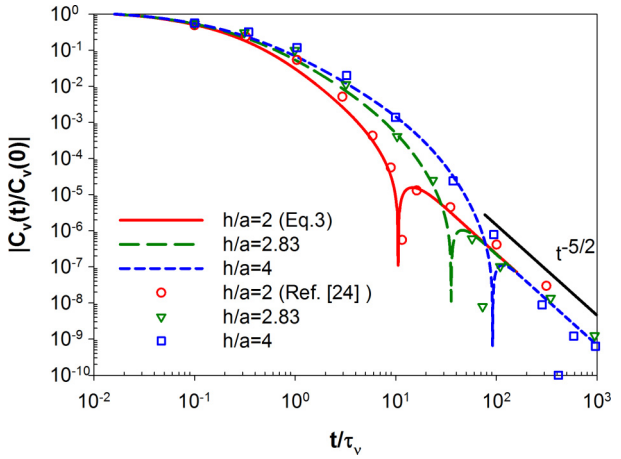

FIG. 6. (Color online) Normalized VACF of a non-neutrally buoyant Brownian particle near an infinite plane wall in an incompressible, quiescent fluid medium for different separations from the wall. The symbols are the corresponding results from Ref. [24]. $\rho_p/\rho = 2.25$ with ρ_p being the density of the particle.

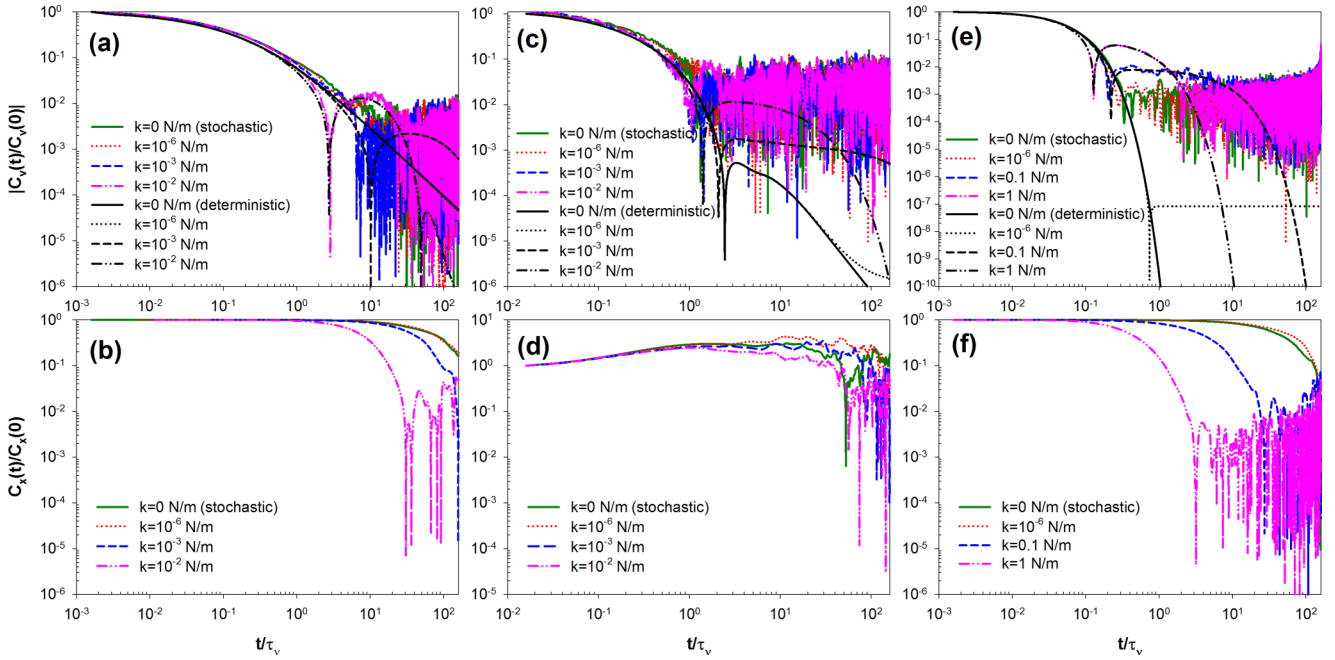

FIG. 7. (Color online) Normalized VACF and PACF of a neutrally buoyant Brownian particle at different locations subject to harmonic potentials of different strengths: (a) VACF in an unbounded (bulk) fluid, (b) PACF in an unbounded fluid, (c) VACF for $h/a = 2$, (d) PACF for $h/a = 2$, (e) VACF for $h/a = 1.14$, and (f) PACF for $h/a = 1.14$. For the VACF, both stochastic and deterministic solutions are shown for comparison.

presence of a harmonic spring for different particle positions relative to the wall. For a particle in the bulk [Figs. 7(a) and 7(b); 100 stochastic simulations with $\Delta t = 10^{-10}$ s] and near the wall with $h/a = 2$ [Figs. 7(c) and 7(d); 2000 stochastic simulations with $\Delta t = 10^{-9}$ s], the chosen spring constant is consistent with an optical trap or adhesion with polymer tethers [Figs. 1(b) and 1(c)]; for a particle in the lubrication layer [Figs. 7(e) and 7(f); 200 realizations with $\Delta t = 10^{-10}$ s] the spring constant is chosen for an optical trap or ligand-receptor binding [Figs. 1(b) and 1(d)]. Similar to Fig. 5, our stochastic and deterministic solutions in $C_v(t)$ agree for different h/a and k, justifying the self-consistency of our method. When the particle is bound by a spring, a second time scale, $\tau_k = 2\pi\sqrt{\frac{m}{k}}$, characterizing the spring vibration frequency comes into play. As is noticeable in Fig. 7, oscillations in $C_v(t)$ occur due to the spring mechanical force, with the minimum of the oscillation being observed at $t \sim \tau_k$. It is expected that at much longer times when the spring force $-kx$ balances the drag force $6\pi\eta aU$, $C_v(t)$ would exhibit the $t^{-7/2}$ scaling for a particle in the bulk and $t^{-9/2}$ scaling for a particle near a wall at $t \gtrsim \frac{6\pi\eta a}{k}$ [24]. We note that the cases of $k = 10^{-2}$ N/m in Figs. 7(a) and 7(c) already exhibit the expected final $t^{-7/2}$ and $t^{-9/2}$ correlations at $t/\tau_v > 10^2$. In order to resolve this correlation for weaker springs, longer simulations are necessary. The comparison of τ_k to τ_v for different k values is summarized in Table I. The corresponding correlation of particle displacement $C_x(t)$ decays at the time scale where the particle velocity starts to decorrelate with its initial value. Therefore, in the presence of the spring, the decrease of $C_x(t)$ is prominent at $t \sim \tau_k$. As indicated in Sec. III, due to the mathematical nonstationarity of the composite GLE for $h/a = 2$, in Fig. 7(d) the ensemble average of $\langle \delta x(t)\delta x(0)\rangle$ is essentially equivalent to $\langle \delta x(t)\rangle$. Consequently, for a particle initially placed at the harmonic potential minimum, C_x first increases and then decreases as $U_\perp(t)$ changes sign.

In order to further validate our GLE results for a bound nanoparticle in the lubrication regime, which is pertinent to nanocarrier adhesion encountered in targeted drug delivery, we compare the GLE results with the DNS results [18,45] for $h/a = 1.14$ and $k = 1$ N/m in Fig. 8(a). The stochastic solutions for DNS (25 realizations, $\Delta t = 10^{-10}$ s) are obtained using the fluctuating hydrodynamics approach [15,18] with the finite element method where the particle is immersed in a fluctuating Navier-Stokes fluid within a cylindrical channel of radius $R = 10a$. Meanwhile, we calculate the nonfluctuating counterpart of the particle motion using DNS and obtain the deterministic solutions for a particle initially driven by a weak force. Strikingly, our GLE results for $k = 1$ N/m in Figs. 7(e) and 8(a) agree well with the corresponding DNS results, which validates the general applicability of our quasisteady-state lubrication assumption in Eq. (4) when a strong adhesion is present. The slightly earlier spring oscillation and the absence of a second oscillation due to the wall for the GLE results are caused by the absence of wall curvature and the neglect of

TABLE I. Comparison of the spring time scale to the viscous relaxation time.

k (N/m)	τ_k (s)	τ_k/τ_v
1	5.08×10^{-8}	0.813
0.1	1.61×10^{-7}	2.572
10^{-2}	5.08×10^{-7}	8.133
10^{-3}	1.61×10^{-6}	25.719
10^{-6}	5.08×10^{-5}	813.306

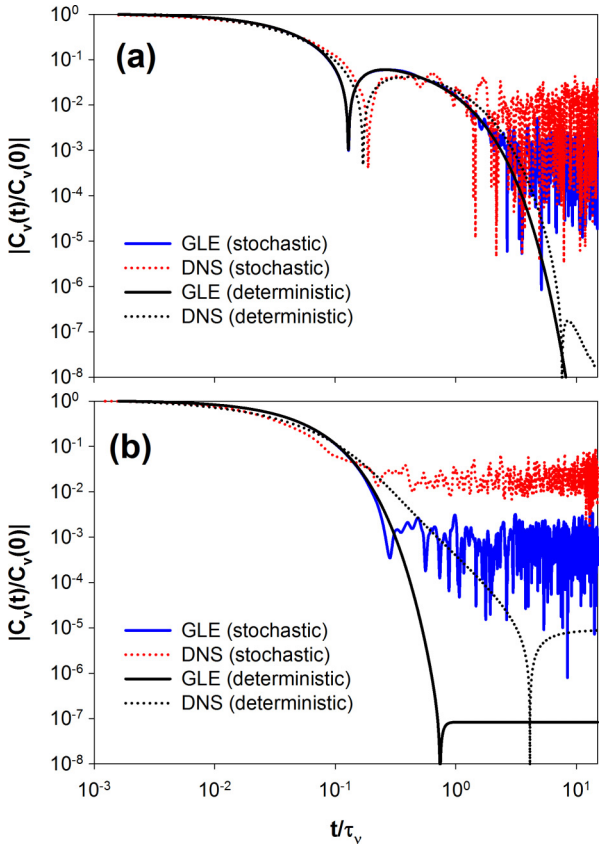

FIG. 8. (Color online) Normalized VACF of a neutrally buoyant Brownian particle in the lubrication regime with $h/a = 1.14$ in the presence of (a) a strong adhesion with $k = 1$ N/m and (b) a weak trapping force obtained from GLE and DNS.

fluid transient diffusion in Eq. (4). In the absence of adhesion or when the particle is only trapped by a weak force [Fig. 8(b); $k = 0$ or 10^{-6} N/m], the deviation between GLE and DNS becomes more apparent due to the lack of an appropriate memory kernel. In such a case, one may invoke a composite GLE that incorporates the suitable power-law correlations obtained from DNS.

C. Milestoning rate from the reactive flux formalism

Invoking the reactive flux formalism [25], the effect of hydrodynamics on the kinetics of a particle originating from $x < x_m$ crossing a predefined milestone x_m can be characterized through the correlation for characteristic state functions: $k_{corr}(t) \equiv \frac{\langle h_A[x(0)]\dot{h}_B[x(t)]\rangle}{\langle h_A[x(0)]\rangle} = \frac{d}{dt}\frac{\langle h_A[x(0)]h_B[x(t)]\rangle}{\langle h_A[x(0)]\rangle}$, where $h_A = 1$ if $|x| \leqslant x_m$ and $h_A = 0$ if $|x| > x_m$; $h_B = 0$ if $|x| \leqslant x_m$ and $h_B = 1$ if $|x| > x_m$. A typical milestoning correlation function shows an initial value of k followed by a relaxation process characterized by a time scale of τ_m (Fig. 9). Here $k_m(s^{-1}) = k_{corr}(t = 0)$ is the rate of a particle passing the milestone, and $\tau_m(s)$ is the time scale when the net flux of a particle passing the milestone goes to zero. We choose τ_m to be the time at which $k_{corr}(t)$ decays to less than 5% of k_m. Figure 10(a) compares the milestoning rate for various particle positions, spring constants, and milestones of the harmonic potential. If the milestoning process is dominated by particle diffusion (black histograms), $k_m \propto D$. Distinct from

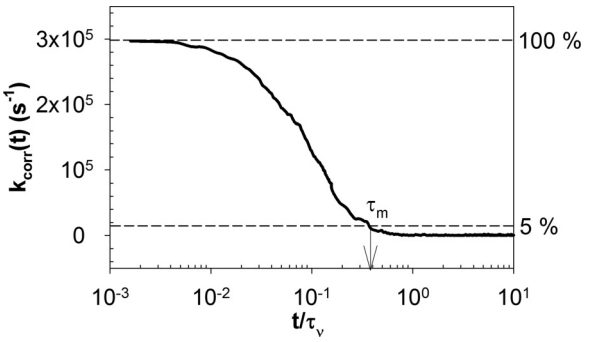

FIG. 9. Milestoning correlation function $k_{corr}(t)$ for $h/a = 1.14$, $k = 1$ N/m, and $x_m = 2$Å (corresponding to the energy of 4.68 k_BT within the harmonic potential). The dashed lines indicate dropping of k_m from 100% to 5%, and the arrow indicates the determination of τ_m.

the expected trend for the scaled diffusivity for a particle at different positions from the wall (inset), the result indicates that the lubrication force enhances k_m as the upward force pushes the particle away from the equilibrium position and facilitates the rate of milestone crossing. The reconstructed graph for the scaled k_m with different spring constants [Fig. 10(b)] shows that k_m roughly scales as $k^{1/2}$, the intuitive result determined by the vibration rate of a particle within a harmonic potential (dashed line). The spreading of the data (i.e., the deviations from the dashed line) across different milestones and hydrodynamic regimes emphasizes the effect of fluid viscous dissipation. Because the hydrodynamic time scale for the lubrication force is smaller than that in the bulk, the more distinct separation of hydrodynamic and spring time scales makes the spring effect decoupled from the hydrodynamics. It is, therefore, not surprising that when the particle is in the lubrication regime, k_m conforms more with the $k^{1/2}$ scaling. The similar scaling for the equilibration frequency τ_m^{-1} shown in Fig. 10(c) suggests that $k_m \propto \tau_m^{-1}$, and our determination of these two characteristic parameters for milestoning without a reaction coordinate is self-consistent.

V. CONCLUSION

In conclusion, we introduced a composite GLE as a feasible unified framework for predicting the particle dynamics in the presence of thermal fluctuations across different hydrodynamic and adhesion regimes. Analyzing particle trajectories generated from the stochastic simulations of the composite GLE allows us to extract the particle autocorrelation functions of velocity and position, which dictate how the particle responds to instantaneous hydrodynamic resistance, Brownian force, and the thermodynamic driving force originated from the adhesive energy landscape. In the spirit of the reactive flux formalism, we characterize the milestoning correlation function and find that both wall-hydrodynamics and adhesive forces have significant impact on the kinetics of a particle crossing a specific milestone. Specifically, weaker hydrodynamic resistance or softer binding potential yield a smaller milestoning rate. This effect is critical when simultaneous binding and rolling of nanoparticles and cells occur such as in targeted drug delivery or during the mounting of an immune response. Generalizing the methodology, we envision

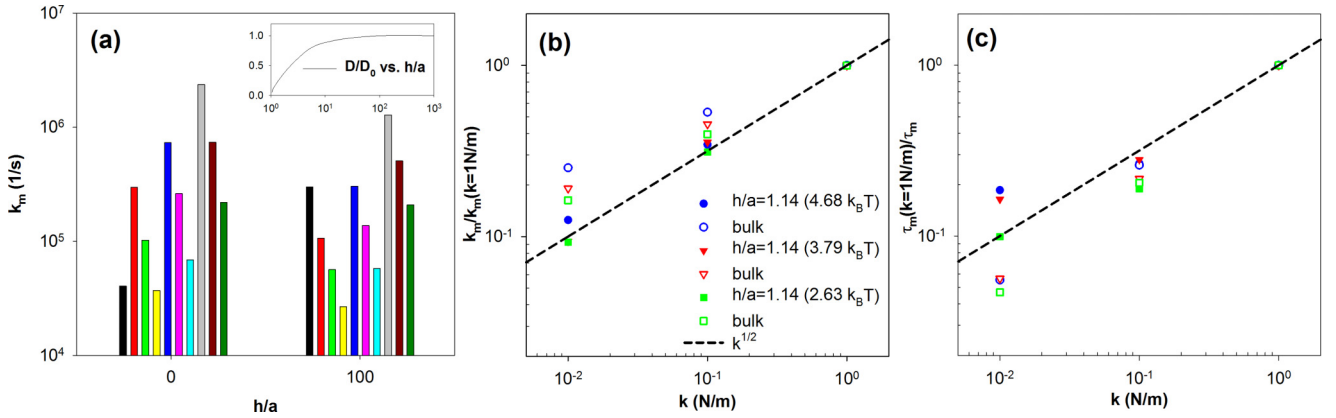

FIG. 10. (Color online) (a) Milestoning rate $k_m(1/s)$ for different particle separations from the wall, spring constants, and milestones. $h/a = 100$ corresponds to a particle in an unbounded fluid. Black (control): purely diffusive expectation where the histogram for the bulk is obtained by averaging all the k_m values for the bulk, and the histogram for $h/a = 1.14$ is obtained by multiplying the bulk result by $\beta^{-1} = (h-a)/a$. Other histograms from left to right: $F_m = 4.68k_BT$ and $k = 1$ N/m (red), $k = 0.1$ N/m (light green), $k = 0.01$ N/m (yellow); $F_m = 3.79k_BT$ and $k = 1$ N/m (dark blue), $k = 0.1$ N/m (pink), and $k = 0.01$ N/m (cyan); $F_m = 2.68k_BT$ and $k = 1$ N/m (grey), $k = 0.1$ N/m (dark red), $k = 0.01$ N/m (dark green). The inset shows the scaled diffusivity β^{-1} for a purely diffusive Brownian particle at different h/a. (b) The scaled milestoning rate $k_m/k_m(k = 1$ N/m) as a function of spring constant for different configurations. The dashed line corresponds to the scaling for purely mechanical motion of a particle without any viscous damping. (c) Scaled equilibration frequency $\tau_m(k = 1$ N/m)$/\tau_m$ as a function of spring constant for different configurations. The symbol and line descriptions are the same as (b).

that when the particle is subject to a complex energy landscape with the milestone being chosen to be a true transition state, the proposed formalism can characterize the effect of hydrodynamic interactions on attachment-detachment kinetics involved in mono- and multivalent binding.

ACKNOWLEDGMENTS

The GLE aspect of this work was supported in part by the National Institutes of Health (NIH) grant R01 EB006818, and the reactive flux aspect was supported by the NIH Grant U01 EB016027. We acknowledge shared resources provided by XSEDE (Grant No. MCB060006) and NSF DMR 1120901.

APPENDIX A: NUMERICAL INTEGRATION OF GENERALIZED LANGEVIN EQUATIONS

Equations (2)–(4) can be cast in the form of

$$\frac{d^2x}{dt^2} = -\Theta_1(t)\frac{dx}{dt} - \Theta_2(t)\int_0^t |t-t'|^{-\lambda}\frac{dx}{dt'}dt' - \Theta_3(t)x + \Theta_4(t) \tag{A1}$$

with the initial conditions $x(0) = 0$, $\frac{dx}{dt}|_{t=0} = U(0) = \sqrt{\frac{k_BT}{M}}$, and $\frac{d^2x}{dt^2}|_{t=0} = U'(0) = 0$. If we express the derivatives using finite differences, the corresponding explicit discretized equation reads

$$\frac{x_{i+1} - 2x_i + x_{i-1}}{(\Delta t)^2} = -\Theta_{1,i}\frac{x_{i+1} - x_{i-1}}{2\Delta t} - \Theta_{2,i}\sum_{j=1}^{i-1}\left[|(i-j)\Delta t|^{-\lambda}\left(\frac{x_{j+1} - x_{j-1}}{2\Delta t}\right)\Delta t\right] - \Theta_{3,i}x_i + \Theta_{4,i}, \tag{A2}$$

where Δt is the time step size and we have changed the lower limit of integration from $-\infty$ to 0 as the numerical integration would be counted from time zero. The initial conditions are $x_1 = 0$ and $x_0 = -U(0)\Delta t$, $x_{-1} = -2U(0)\Delta t \cdots$ for times earlier than the initial time of numerical integration. This explicit scheme with a fixed Δt allows us to directly make use of x_j and U_j for $j \leqslant i$ efficiently. In the following subsections, we delineate the numerical schemes for Eqs. (2)–(3) with a memory kernel and Eq. (4) separately.

In all three cases, we follow the Ito calculus for integrating stochastic differential equations and neglect the "drift" due to the spatially dependent drag $\zeta(x)$ (or the corresponding spatially dependent particle diffusivity $D(x) = \frac{k_BT}{\zeta(x)}$). We have also modified the equation of motion for the lubrication case by including an additional drift $[= \zeta(x)\frac{dD(x)}{dx} = -\frac{k_BT}{\zeta(x)}\frac{d\zeta}{dx}]$ [46], the results are nearly identical to those without the drift considered.

1. Brownian Particle in an Unbounded Fluid Domain: Eq. (2)

Comparing terms on the right-hand side of Eq. (A1), clearly the scheme may be unstable when $\lambda > 1$ and $\Delta t \ll 1$ as Θ and (dx/dt) are finite. To avoid this issue in integrating Eq. (2) with $\lambda = 3/2$, the memory kernel term in Eq. (A1) is integrated by

parts to yield

$$\frac{d^2x}{dt^2} = -\Theta_1(t)\frac{dx}{dt} - \frac{\Theta_2(t)}{1-\lambda}t^{1-\lambda}\frac{dx}{dt'}\bigg|_{t'=0} - \frac{\Theta_2(t)}{1-\lambda}\int_0^t |t-t'|^{1-\lambda}\frac{d^2x}{dt'^2}\,dt' - \Theta_3(t)x + \Theta_4(t) \tag{A3}$$

with $|t-t'|^{1-\lambda}\left(dx/dt'\right)\big|_{t'=t} \to 0$. In its discretized form, we have

$$\left[1+\frac{\Theta_{1,i}}{2}\Delta t\right]x_{i+1} = [2-\Theta_{3,i}(\Delta t)^2]x_i - \left[1-\frac{\Theta_{1,i}}{2}\Delta t\right]x_{i-1} - \frac{\Theta_{2,i}}{1-\lambda}|i\Delta t|^{1-\lambda}U(0)(\Delta t)^2$$
$$- \frac{\Theta_{2,i}}{1-\lambda}\sum_{j=1}^{i-1}[|(i-j)\Delta t|^{1-\lambda}(x_{j+1}-2x_j+x_{j-1})\Delta t] + \Theta_{4,i}(\Delta t)^2. \tag{A4}$$

2. Brownian Particle Near a Planar Bounding Wall: Eq. (3)

When $2<\lambda<3$ as seen in Eq. (3), a second integration by parts for the memory kernel is required. Thus we obtain the form of

$$\frac{d^2x}{dt^2} = -\Theta_1(t)\frac{dx}{dt} - \frac{\Theta_2(t)}{1-\lambda}t^{1-\lambda}\frac{dx}{dt'}\bigg|_{t'=0} - \frac{\Theta_2(t)}{(1-\lambda)(2-\lambda)}t^{2-\lambda}\frac{d^2x}{dt'^2}\bigg|_{t'=0}$$
$$- \frac{\Theta_2(t)}{(1-\lambda)(2-\lambda)}\int_0^t |t-t'|^{2-\lambda}\frac{d^3x}{dt'^3}\,dt' - \Theta_3(t)x + \Theta_4(t), \tag{A5}$$

where both $|t-t'|^{1-\lambda}(dx/dt')|_{t'=t}$ and $|t-t'|^{2-\lambda}(d^2x/dt'^2)|_{t'=t}$ go to zero. To further ensure the numerical stability for Eq. (3) as the integral-differential equation has a more complex structure, in the spirit of Crank-Nicholson method we break the memory kernel integration into t_{i+1} and t_i terms along with finite difference discretization, and arrive at

$$\frac{x_{i+1}-2x_i+x_{i-1}}{(\Delta t)^2} = -\Theta_{1,i}\frac{x_{i+1}-x_{i-1}}{2\Delta t} - \frac{\Theta_{2,i}}{1-\lambda}|i\Delta t|^{1-\lambda}U(0) - \frac{\Theta_{2,i}}{(1-\lambda)(2-\lambda)}|i\Delta t|^{2-\lambda}U'(0)$$
$$- \frac{\Theta_{2,i}}{(1-\lambda)(2-\lambda)}\left\{\sum_{j=1}^{i}|(i+1-j)\Delta t|^{2-\lambda}\left[\frac{x_{j+1}-3x_j+3x_{j-1}-x_{j-2}}{\Delta t^2}\right]\right.$$
$$\left. + \sum_{j=0}^{i-1}|(i-j)\Delta t|^{2-\lambda}\left[\frac{x_{j+1}-3x_j+3x_{j-1}-x_{j-2}}{\Delta t^2}\right]\right\} - \Theta_{3,i}x_i + \Theta_{4,i} \tag{A6}$$

or

$$x_{i+1} = \left[1+\frac{\Theta_{1,i}\Delta t}{2}+\frac{\Theta_{2,i}(\Delta t)^{2-\lambda}}{2(1-\lambda)(2-\lambda)}\right]^{-1}\left\{\left[2+\frac{3\Theta_{2,i}(\Delta t)^{2-\lambda}}{2(1-\lambda)(2-\lambda)}-\Theta_{3,i}(\Delta t)^2\right]x_i - \left[1-\frac{\Theta_{1,i}}{2}\Delta t+\frac{3\Theta_{2,i}(\Delta t)^{2-\lambda}}{2(1-\lambda)(2-\lambda)}\right]x_{i-1}\right.$$
$$+\frac{\Theta_{2,i}(\Delta t)^{2-\lambda}}{2(1-\lambda)(2-\lambda)}x_{i-2} - \frac{\Theta_{2,i}}{1-\lambda}|i\Delta t|^{1-\lambda}U(0)(\Delta t)^2 - \frac{\Theta_{2,i}}{(1-\lambda)(2-\lambda)}\sum_{j=1}^{i-1}[|(i+1-j)\Delta t|^{2-\lambda}(x_{j+1}-3x_j+3x_{j-1}-x_{j-2})]$$
$$\left. - \frac{\Theta_{2,i}}{(1-\lambda)(2-\lambda)}\sum_{j=0}^{i-1}[|(i-j)\Delta t|^{2-\lambda}(x_{j+1}-3x_j+3x_{j-1}-x_{j-2})] + \Theta_{4,i}(\Delta t)^2\right\} \tag{A7}$$

as $U'(0)=0$.

3. Brownian Particle Extremely Close to a Planar Bounding Wall: Eq. (4)

In the absence of the memory kernel, $\Theta_2 = 0$, and Eq. (A1) can be numerically integrated using finite difference alone:

$$\left[1+\frac{\Theta_{1,i}}{2}\Delta t\right]x_{i+1} = [2-\Theta_{3,i}(\Delta t)^2]x_i - \left[1-\frac{\Theta_{1,i}}{2}\Delta t\right]x_{i-1} + \Theta_{4,i}(\Delta t)^2. \tag{A8}$$

APPENDIX B: NOISE GENERATION FOR $R(t)$

The fluctuations in Eqs. (2)–(4) are determined through random number generation. For fluctuations with a δ-function correlation, we first generate Gaussian white noise ξ_i that has zero mean and unit variance. R_i is then obtained by $R_i = \xi_i\sqrt{\zeta_0/\Delta t}$ to preserve $\langle R_i^2\rangle = \zeta_0/\Delta t$ and $\langle R_i\rangle = 0$ for a desired prefactor ζ_0. For fluctuations with a power-law

correlation of index λ, we apply an approximate method delineated in Refs. [41,42] to generate series of colored random numbers. Briefly, the prescribed noise spectrum is introduced in the frequency f (inverse-time) domain by taking the following procedures:

(1) Generate Gaussian white noise ξ_i for $i = 1 \sim N$ if the total number of time steps is N.

(2) Fourier transform ξ_i to obtain $\hat{\xi}_i = F\{\xi_i\}$.

(3) Introduce the colored correlation by multiplying $\hat{\xi}_i$ by $f_i^{(\lambda-1)/2}$.

(4) Inverse Fourier transform to obtain $\xi_{\lambda,i} = F^{-1}\{\hat{\xi}_i f_i^{(\lambda-1)/2}\}$ with $\langle \xi_{\lambda,i}\xi_{\lambda,j}\rangle \propto |i-j|^{\lambda}$.

(5) First normalize $\xi_{\lambda,i}$ and rescale it to obtain $\langle R_i R_j\rangle = \zeta_0|(i-j)\Delta t|^{-\lambda}$ and $\langle R_i\rangle = 0$.

As seen from Fig. 11, the normalized noise autocorrelation function C_R, $\langle R_1 R_i\rangle / \langle R_1 R_1\rangle$, for 20 realizations satisfies the prescribed scaling, $|i\Delta t|^{-\lambda}$.

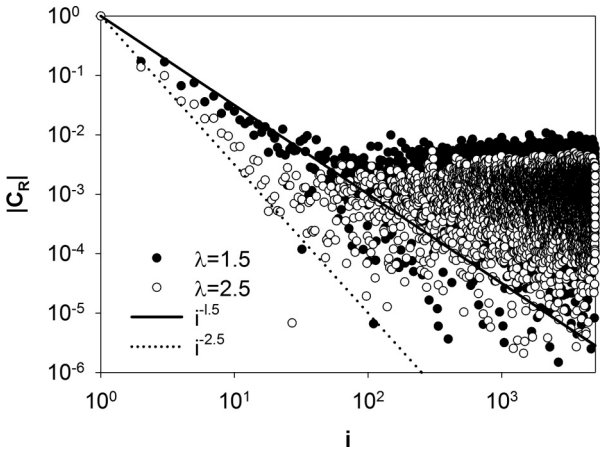

FIG. 11. Noise autocorrelation function for $\lambda = 1.5$ and 2.5. Symbols are simulated results, and lines are the prescribed scalings.

[1] D. Peer, J. M. Karp, S. Hong, O. C. Farokhzad, R. Margalit, and R. Langer, Nat. Nanotechnol. **2**, 751 (2007).

[2] Z. Cheng, A. A. Zaki, J. Z. Hui, V. R. Muzykantov, and A. Tsourkas, Science **338**, 903 (2012).

[3] P. S. Ayyaswamy, V. Muzykantov, D. M. Eckmann, and R. Radhakrishnan, J. Nanotechnol. Eng. Med. **4**, 011001 (2013).

[4] N. V. Zaytseva, V. N. Goral, R. A. Montagna, and A. J. Baeumner, Lab Chip **5**, 805 (2005).

[5] R. Riahi, K. E. Mach, R. Mohan, J. C. Liao, and P. K. Wong, Anal. Chem. **83**, 6349 (2011).

[6] A. Huebner, M. Srisa-Art, D. Holt, C. Abell, F. Hollfelder, A. J. deMello, and J. B. Edel, Chem. Commun. **12**, 1218 (2007).

[7] G. Rigaut, A. Shevchenko, B. Rutz, M. Wilm, M. Mann, and B. Séraphin, Nat. Biotechnol. **17**, 1030 (1999).

[8] M. P. MacDonald, G. C. Spalding, and K. Dholakia, Nature (London) **426**, 421 (2003).

[9] M. M. Wang, E. Tu, D. E. Raymond, J. M. Yang, H. Zhang, N. Hagen, B. Dees, E. M. Mercer, A. H. Forster, I. Kariv, P. J. Marchand, and W. F. Butler, Nat. Biotechnol. **23**, 83 (2005).

[10] A.-E. Saliba, L. Saias, E. Psychari, N. Minc, D. Simon, F.-C. Bidard, C. Mathiot, J.-Y. Pierga, V. Fraisier, J. Salamero, V. Saada, F. Farace, P. Vielh, L. Malaquin, and J.-L. Viovy, Proc. Natl. Acad. Sci. U. S. A. **107**, 14524 (2010).

[11] H. A. Nieuwstadt, R. Seda, D. S. Li, J. B. Fowlkes, and J. L. Bull, Biomed. Microdevices **13**, 97 (2011).

[12] D. T. Chen, E. R. Weeks, J. C. Crocker, M. F. Islam, R. Verma, J. Gruber, A. J. Levine, T. C. Lubensky, and A. G. Yodh, Phys. Rev. Lett. **90**, 108301 (2003).

[13] R. R. Brau, J. M. Ferrer, H. Lee, C. E. Castro, B. K. Tam, P. B. Tarsa, P. Matsudaira, M. C. Boyce, R. D. Kamm, and M. J. Lang, J. Opt. A: Pure Appl. Opt. **9**, S103 (2007).

[14] D. Wirtz, Annu. Rev. Biophys. **38**, 301 (2009).

[15] B. Uma, T. N. Swaminathan, R. Radhakrishnan, D. M. Eckmann, and P. S. Ayyaswamy, Phys. Fluids **23**, 073602 (2011).

[16] B. Uma, T. N. Swaminathan, P. S. Ayyaswamy, D. M. Eckmann, and R. Radhakrishnan, J. Chem. Phys. **135**, 114104 (2011).

[17] B. Uma, D. M. Eckmann, P. S. Ayyaswamy, and R. Radhakrishnan, Mol. Phys. **110**, 1057 (2012).

[18] R. Radhakrishnan, B. Uma, J. Liu, P. S. Ayyaswamy, and D. M. Eckmann, J. Comp. Phys. **244**, 252 (2013).

[19] D. L. Ermak and J. A. McCammon, J. Chem. Phys. **69**, 1352 (1978).

[20] J. F. Brady, Ann. Rev. Fluid Mech. **20**, 111 (1988).

[21] J.-P. Hansen and I. R. McDonald, *Theory of Simple Liquids*, 3rd ed. (Academic Press, London, 2006).

[22] B. U. Felderhof, J. Phys. Chem. B **109**, 21406 (2005).

[23] J. T. Padding and A. A. Louis, Phys. Rev. E **74**, 031402 (2006).

[24] T. Franosch and S. Jeney, Phys. Rev. E **79**, 031402 (2009).

[25] D. Chandler, J. Chem. Phys. **68**, 2959 (1978).

[26] S. Jeney, B. Lukić, J. A. Kraus, T. Franosch, and L. Forró, Phys. Rev. Lett. **100**, 240604 (2008).

[27] H. Jensenius and G. Zocchi, Phys. Rev. Lett. **79**, 5030 (1997).

[28] F. Oesterhelt, M. Rief, and H. E. Gaub, New J. Phys. **1**, 6 (1999).

[29] R. Kubo, Rep. Prog. Phys. **29**, 255 (1966).

[30] L. D. Landau and E. M. Lifshitz, *Fluid Mechanics* (Pergamon, London, 1959).

[31] R. Zwanzig and M. Bixon, Phys. Rev. A **2**, 2005 (1970).

[32] J. D. Schieber, A. Córdoba, and T. Indei, J. Non-Newtonian Fluid Mech. **200**, 3 (2013).

[33] T. Gotoh and Y. Kaneda, J. Chem. Phys. **76**, 3193 (1982).

[34] M. H. J. Hagen, I. Pagonabarraga, C. P. Lowe, and D. Frenkel, Phys. Rev. Lett. **78**, 3785 (1997).

[35] I. Pagonabarraga, M. H. J. Hagen, C. P. Lowe, and D. Frenkel, Phys. Rev. E **58**, 7288 (1998).

[36] H. A. Lorentz, Abh. Theor. Physik **1**, 23 (1907).

[37] J. Liu, G. E. R. Weller, B. Zern, P. S. Ayyaswamy, D. M. Eckmann, V. R. Muzykantov, and R. Radhakrishnan, Proc. Natl. Acad. Sci. U. S. A. **107**, 16530 (2010).

[38] D. Frydel and S. A. Rice, Phys. Rev. E **76**, 061404 (2007).

[39] R. Tatsumi and R. Yamamoto, J. Chem. Phys. **138**, 184905 (2013).

[40] G. L. Leal, *Advanced Transport Phenomena* (Cambridge University Press, New York, 2007).

[41] A. V. Chechkin and V. Y. Gonchar, Chaos Solitons Fractals **12**, 391 (2001).

[42] O. Y. Sliusarenko, V. Y. Gonchar, A. V. Chechkin, I. M. Sokolov, and R. Metzler, Phys. Rev. E **81**, 041119 (2010).

[43] D. Chandler, *Introduction to Modern Statistical Mechanics* (Oxford University Press, New York, 1987).

[44] D. Frenkel and B. Smit, *Understanding Molecular Simulation: From Algorithms to Applications*, 2nd ed. (Academic Press, New York, 2002).

[45] H. Vitoshkin, H.-Y. Yu, D. M. Eckmann, P. S. Ayyaswamy, and R. Radhakrishnan (unpublished).

[46] A. W. C. Lau and T. C. Lubensky, Phys. Rev. E **76**, 011123 (2007).